CROR blade deformation, part 1: Experimental results by strain pattern analysis

A. Geeraert, C. Stephan

CROR BLADE DEFORMATION, PART 1:

EXPERIMENTAL RESULTS BY STRAIN PATTERN ANALYSIS

A. GEERAERT[1], C. STEPHAN[1]

[1] ONERA
The French Aerospace Lab, 92322 Châtillon, FRANCE
arnaud.geeraert@onera.fr

Keywords: CROR, aeroelastic deformation, experimental measurement, SPA.

Abstract: Although contra-rotating open rotors (CROR) were experimented mainly in the 40's, even limitedly produced in some countries, and with enhanced performances compared to single propellers, their complex design, installation and maintenance prevented them from being used over an extended period of time. The current research by aeronautical community on bringing significant step changes regarding the environmental impact of aviation has given new impetus to this kind of propulsion system. Within the CleanSky SFWA-ITD project, recent wind tunnel tests campaigns have been performed to get a deeper understanding of the complex phenomena involving aerodynamic, acoustic, structural, performances, and aeroelastic topics.

Concerning particularly the latter topic, this European project has been an opportunity to improve both experimental and numerical methods to estimate operational blade deformation. The whole achieved work is described in two companion papers.

This first paper presents the preparation and application of the Strain Pattern Analysis (SPA) during the Z49 CROR wind tunnel tests, with Airbus AI-PX7 generic blades [1], as the experimental method used to determine the steady and unsteady blade deformations over all azimuths by recombination of reduced number of modal shapes. The important initial step of optimising the strain gauges bridges locations by maximising the structural modes observability and minimising the information redundancy shared by a set of sensors is detailed. Instrumentation constraints taken into account are listed to highlight the difficulty of applying the SPA with such composite structures. Then a numerical sensitivity study, from which results are exposed, has been performed before manufacturing the blades to determine the optimal set of SPA parameters and to evaluate the expected error induced by SPA on a reference case in cruise conditions. The next phase concerning the laboratory tests results is detailed, describing the calibration of the instrumented blades, the instrumentation verification in non-rotating and rotating conditions, as well as a first validation of the SPA of blades subject to a distributed static loading. The final experimental step concerns the application of SPA during the wind tunnel tests (WTT) at ONERA S1MA facility, from signal pre-processing to typical final results, such as steady and unsteady bending and twist, useful for a better understanding of the blades aeroelastic behaviour and CROR performances.

A companion paper [7] describes the improvement of numerical methods to calculate the blades aeroelastic deformation and compares the obtained numerical results with experimental SPA results mentioned here-above.

1 INTRODUCTION

Within the Joint Technology Initiative “JTI CleanSky”, the Smart Fixed Wing Aircraft Integrated Technology Demonstrator “SFWA-ITD” project addresses, among many other items, the integration of novel components such as innovative power-plants with special focus on contra-rotating open rotors, aiming at reducing significantly the fuel burn of aircrafts.

The Z49 CROR evaluation, led by Airbus, has reached an important milestone with the wind tunnel tests campaign in ONERA S1MA facility. Among various quantities allowing to analyse the behaviour and to estimate the performances of this CROR configuration, the steady and unsteady blade deformations have been obtained thanks to the implementation of the Strain Pattern Analysis (SPA) by the ONERA Aeroelasticity and Structural Dynamics Department on one front blade and one rear blade.

Figure 1 – Z49 CROR in ONERA S1MA WTT

2 THE STRAIN PATTERN ANALYSIS

Measuring deflections of a moving structure is of high interest but may turn out to be quite difficult. This is especially true for rotating structures, where most of optical measurement systems, although non-intrusive, reach their limits quickly in terms of visualisation azimuthal range and data acquisition frequency and/or duration. A solution to address this problem is to measure derived quantities such as accelerations or strains. However, although deflections can theoretically be deduced from these quantities by integration and with some assumptions, in practice, a lot of sensors would be needed to reach a guaranteed level of accuracy, and any error in the original measurements would lead to unsound integrated results.

The SPA eliminates any integration. Its principle is to determine the deflection of the structure by combining several modal shapes, as presented in figure 2. The coefficients of the combination, the generalised coordinates, are calculated from strains data, measured from embedded strain gauges at adequate locations in the structure.

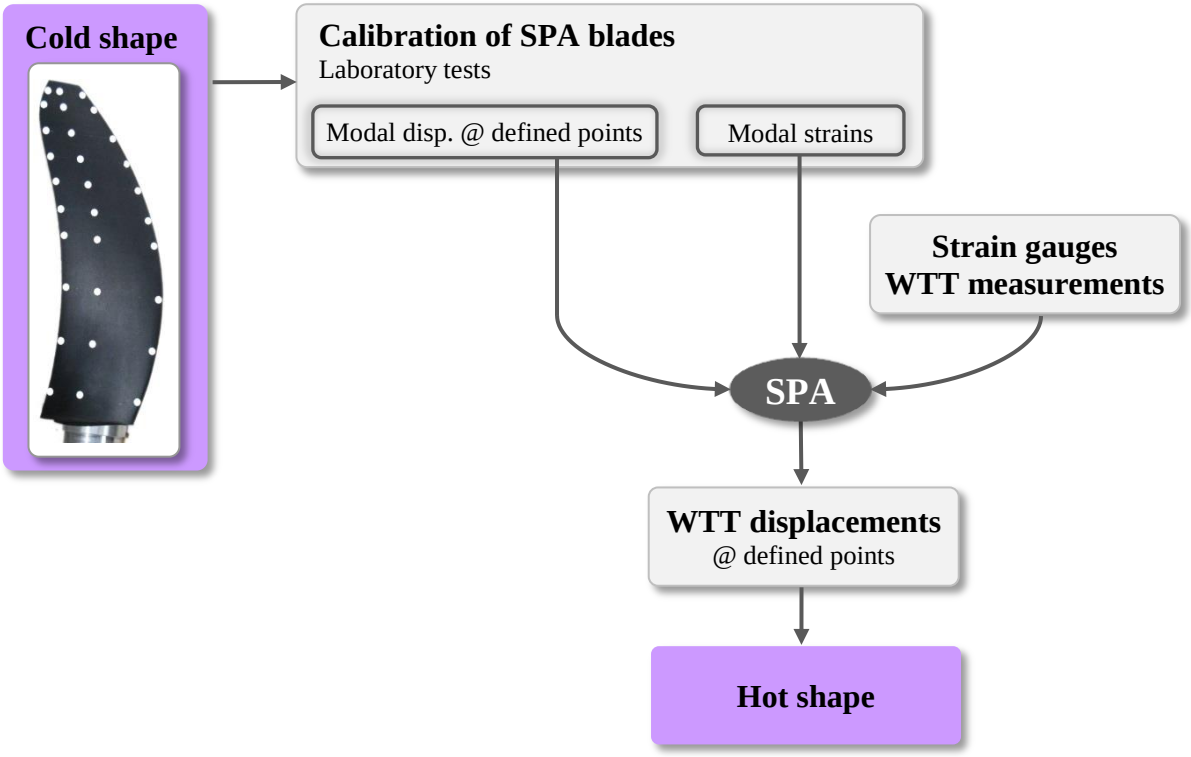

Figure 2 - The Strain Pattern Analysis applied to CROR WTT

2.1 Calibration phase

The first step for applying SPA is a calibration phase which consists in a ground vibration test (GVT) of the studied structure without rotating movement. Using a Phase Resonance Method (PRM), for each k[th] mode of interest, $k \in [1,N]$, deflections and strains are measured simultaneously, accurately giving the corresponding modal shape $\phi_i^{(k)}$ and the modal strain tensor $S_m^{(k)}$, $m \in [1,M]$, from the M strain gauges.

2.2 Main experiment

Then, during the main experiment, which may be ground tests, wind tunnel tests or in-flight tests, strains are recorded as a function of time ($\epsilon_m(t)$, $m \in [1,M]$) and expressed in a reduced modal basis in order to obtain the generalised coordinates ($q^{(k)}(t)$, $k \in [1,N]$). It is shown below that both deflections and strains can be expressed in such a basis with common generalised coordinates, with the assumption of small displacements and deformations.

Theoretically, any displacement can be expressed in a modal basis, assuming that the structure has a linear behaviour (obviously expressing the local modal deflection as a function of the observation point):

$$U_i(x,t) = \sum_{k=1}^{\infty} \phi_i^{(k)}(x) \cdot q^{(k)}(t) \tag{1}$$

The Green-Lagrange strain tensor is defined by (hypothesis of small displacements):

$$\epsilon_{ij}(x,t) = \frac{1}{2}\left(\frac{\partial U_i(x,t)}{\partial x_j} + \frac{\partial U_j(x,t)}{\partial x_i}\right) \tag{2}$$

Finally, replacing (1) into (2), the strain tensor can be expressed as a function of the generalised coordinates:

$$\epsilon_{ij}(x,t) = \sum_{k=1}^{\infty} \frac{1}{2}\left(\frac{\partial \phi_i^{(k)}(x)}{\partial x_j} + \frac{\partial \phi_j^{(k)}(x)}{\partial x_i}\right) \cdot q^{(k)}(t) \tag{3}$$

From (3), the modal strain tensor is identified:

$$S_{ij}^{(k)}(x,t) = \frac{1}{2}\left(\frac{\partial \phi_i^{(k)}(x)}{\partial x_j} + \frac{\partial \phi_j^{(k)}(x)}{\partial x_i}\right) \tag{4}$$

And (3) can be written in a new form:

$$\epsilon_{ij}(x,t) = \sum_{k=1}^{\infty} S_{ij}^{(k)}(x) \cdot q^{(k)}(t) \tag{5}$$

As an infinite number of modes cannot be explored during the calibration phase, a limited number N of modes is fixed, and displacement and strain decomposition can be approximated:

$$U_i(x,t) \approx \sum_{k=1}^{N} \phi_i^{(k)}(x) \cdot q^{(k)}(t) \tag{6}$$

$$\epsilon_{ij}(x,t) \approx \sum_{k=1}^{N} S_{ij}^{(k)}(x) \cdot q^{(k)}(t) \tag{7}$$

The choice of the number N of modes is constrained by the number of embedded strain gauges: to strictly guarantee the distinction of the N modes, N sensors are at least needed. Or in other words, given a number M of sensors, the maximum number of observable modes is M.

Strains are recorded for the M strain gauges in some directions. Thus, (7) can be derived, for the m^{th} strain gauge:

$$\epsilon_m(t) \approx \sum_{k=1}^{N} S_m^{(k)} \cdot q^{(k)}(t) \tag{8}$$

Equation (8) can be written in a matrix form:

$$\epsilon \approx S^T \cdot q \tag{9}$$

And q can be obtained:

$$q \approx (S \cdot S^T)^{-1} \cdot S \cdot \epsilon \tag{10}$$

Rewriting the displacement in a matrix form, this latter is immediately obtained:

$$U_i \approx \phi_i^T \cdot q \tag{11}$$

Obviously, to finally determine accurately the deflection of the structure, great care must be taken when measuring the modal shapes and the modal strains during the calibration phase. But first of all, the locations and orientations of the strain gauges must be judiciously chosen.

3 OPTIMISATION OF THE STRAIN GAUGES LOCATIONS AND ORIENTATIONS

The pattern of the strain gauges is generally deduced from the modes of interest, with pragmatic considerations. Although this leads to a viable pattern, this latter can be optimised to ensure later a more reliable calculation of the structure deflection.

At the beginning of the project, only a predictive Finite Element Model (FEM) was available.

3.1 Optimisation problem definition

An observation equation links the strain gauges outputs $\epsilon_m(t)$ with the modal responses $q^{(k)}(t)$. A general matrix form for this equation is

$$\epsilon = H\{q\} + b \tag{12}$$

with H a functional which can be non-linear or linear and b a time-signal noise process. For the sake of simplicity, b is supposed to be a white noise process. H is often modelled by a linear observability matrix. Hence equation (12) becomes:

$$\epsilon = S^T \cdot q + b \tag{13}$$

which is an extension of (9), including a model of the noise inherent to the recorded time-signal.

The main assumption of the Strain Pattern Analysis is that these modal strain shapes S can form a suitable observability matrix [2-4]. Here the term "suitable" denotes the ability to compute a good estimation of the modal responses $q(t)$ from the measured dynamical strain responses by a least-squares inverse for every discrete time t (equation (10)). It can be noticed that this ability is linked to the linear independence between vectors of S. The goal of an optimised strain gauges positioning is to select the best locations and directions which form the most robust configuration to the level of the noise $b(t)$.

3.2 Optimisation algorithm

The optimisation algorithm is based on a previous accelerometers positioning algorithm developed at the ONERA [5], searching the best sensors pattern with the constraint that two sensors must not provide redundant information. It is proposed here to apply a slightly modified version of this algorithm.

It can be proved that the robustness of the least-squares inverse to the noise is directly linked to the magnitude of the Fisher information matrix I defined by:

$$I = \sum_{k=1}^{N} S_k^T \cdot S_k \tag{14}$$

with S_k the k^{th} row of the modal strain matrix S. A performance measure of a sensors pattern I can be quantified by a matrix norm of I. Unfortunately, several matrix norms exist and a choice must be made. In the literature devoted to the sensors positioning, determinant is usually selected. We prefer to use the spectral radius because it can compute a norm of a defective matrix. Moreover it can estimate the performance of a strain gauges configuration even if there are fewer sensors than modes.

The direct maximisation of I was the final goal of previous sensors positioning methodologies. Traditional sensors positioning algorithms aim to maximise this norm by

iteratively deleting the sensor with the lowest contribution to the sum. Although this maximisation is necessary in order to compute a good estimate of the modal responses, it does not take into account the fact that two potential sensors can have similar information Fisher matrices. Each of them may individually have a major influence on the overall observability. However, if theirs information matrices are close, selecting both sensors may be similar to select one. The redundancy of information between sensors seems to be a pertinent criterion during the determination process of an optimal pattern. Then a constraint is added in order to avoid the redundancy between sensors: each sensor must provide its own information.

It is proposed to quantify the redundancy between two potential gauges by the following formula:

$$R_{kl} = 1 - \frac{\|I_k - I_l\|}{\|I_k + I_l\|} \tag{15}$$

If two potential gauges *k* and *l* have a redundancy R_{kl} close to 1, then they are redundant and only one can be kept. If R_{kl} is close to 0, then each of them brings its own information. This measure is used as a second criterion to select the most relevant positioning for strain gauges.

Finding an optimal sensors pattern becomes the determination of sensors satisfying two constraints:

- they maximise the norm of the information matrix *I*;
- they minimise the redundancy between each couple of strain gauges.

The goal of the proposed strain gauges positioning algorithm is to maximise the Fisher information matrix, with the constraint on the redundancy between strain gauges. If the number of gauges is N_s and the number of potential gauges locations is N_{sc}, then the total number of possible combinations N_c is given by the binomial coefficient:

$$N_c = \frac{N_{sc}!}{(N_{sc} - N_s)!\, N_s!} \tag{16}$$

For a common FEM with several thousand of potential locations, even for a small number of gauges, N_c is a huge number. It is then impossible to test every combination. A sub-optimal algorithm is then required for handling an industrial model. We propose to use an expansion algorithm in two steps:

1. to put the next sensor where it maximises the Fisher information matrix;
2. to delete the sensors which are redundant with this sensor.

This algorithm is stopped when all strain gauges have been put on the structure. In the second step a threshold T_r for the redundancy has to be defined. If the redundancy measure between two sensors is higher than T_r , then they are considered redundant.

3.3 Application to CROR

The final objective of applying SPA to the Z49 CROR wind tunnel tests campaign is to determine the blades deflection accurately enough (maximum displacement error ~ 5%) for a reference case which is defined as follows:

- Mach number = 0.75
- Global incidence = 0°
- Rotation ~ 4500 RPM

- Pt ~ 90000 Pa
- Tt ~ 317 K

Therefore, the optimised strain gauges patterns for both front and rear blades must be defined in order to achieve this objective.

3.3.1 Input data

Insofar as the optimised strain gauges pattern determination must be obviously made prior to manufacturing the blade, the only input data available are predictive FEMs, developed within the CleanSky SFWA-ITD project, comprising approximately of 27000 nodes for the front rear and 20000 nodes for the rear blade. It will be observed a posteriori [7] that these FEMs are representative enough and thus acceptable for being used to optimise the strain gauges locations and orientations.

For information, the first natural modes of the blades are ordered as follows:

Mode	Description
1	First bending
2	Second bending
3	First torsion
4	Third bending
5	Second torsion

Table 1 - Order of blades modes

3.3.2 Constraints on strain gauges positioning

Several pragmatic constraints must be taken into account as inputs of the optimisation process. The most important ones are presented here-below.

The first and severe restriction is the number of recorded channels available for the SPA during experiments. A total of 8 four wires full bridges per blade are allocated, which is quite limited.

To ease the strain gauges installation operation and consequently to limit the possible misorientation, the measurement directions are limited to the span-wise (0°), chord-wise (90°) and shear (45°) directions: the optimisation process deals with discrete parameters and not continuous parameters.

To avoid local delamination of the composite, the overall size of the strain gauges must be small and a minimum distance between two strain gauges must be kept. Additionally, as strain gauges obviously cannot be placed on the external surface of the blades for aerodynamic reasons, they must be placed judiciously in the lay-up.

For correct measurement, the strain gauges must not be placed in areas with high curvature or low thickness, which means that the leading and trailing edges are excluded from the area of acceptable instrumentation.

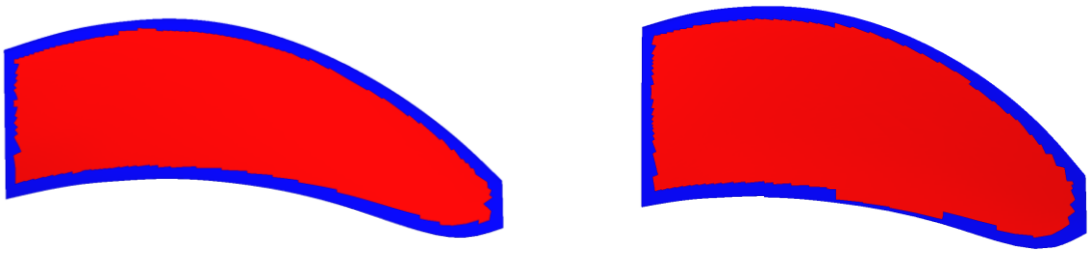

(a) Front blade (b) Rear blade

Figure 3 - Areas of acceptable instrumentation (in red)

3.3.3 Optimised strain gauges patterns

During an optimisation process ruled by the algorithm described in section 3.2, the input parameters are the number of locations for strain gauges placement, the number of modes, and the acceptable directions of strain gauges: span-wise, chord-wise and in-plane shear. The only variable parameter on which we can act is the redundancy threshold, also exposed in section 3.2.

Then, two calculated parameters can be observed as a function of the redundancy in order to help us choosing the best redundancy threshold. The first one is the condition number of the S matrix. It measures the sensitivity of the solution $q(t)$ to noise in the strain gauge recorded time-signals. The closer condition number to 1, the more reliable recalculated deflection.

The second parameter is the Modal Assurance Criterion (MAC) [6] of the modal strains. The MAC of the matrix S depends on the strain gauges placement which also depends on the redundancy level. The best solution is obtained when the modal strains are as differentiable as possible, or in other words, when the off-diagonal terms of the MAC are as low as possible.

For each blade (front & rear), the condition number of the S matrix and the maximum off-diagonal MAC value are plotted as a function of the redundancy level, as shown in figure 4 for examples for the front (3 modes) and rear (5 modes) blades.

Finally, for each blade, the optimised strain gauges pattern is chosen by selecting the redundancy level inducing the lowest condition number and the lowest maximum off-diagonal value.

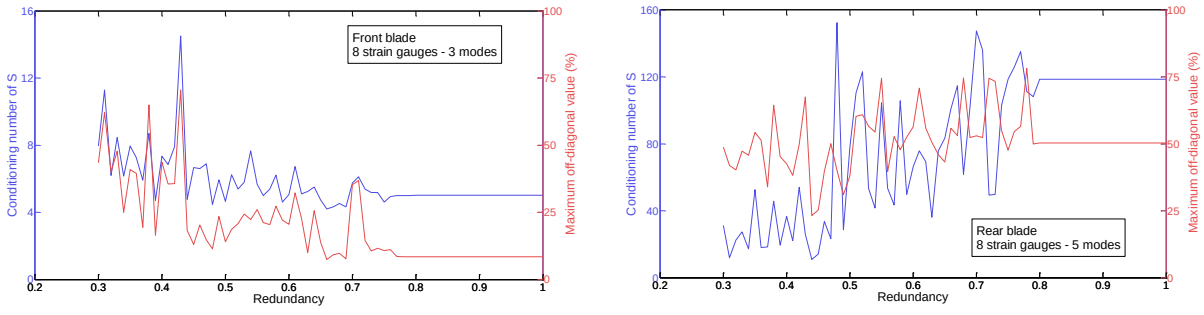

Figure 4 - Selection of optimised strain gauges patterns

The question then arises as to what is the optimum number of modes to be considered in SPA to achieve the objective mentioned above. It might be natural to think that maximising the number of modes would minimise the displacement error. However, a numerical sensitivity study shows that this is not so obvious. By experience, it is well advised to always include the torsion mode(s) in the SPA. Thus, the optimisation process is repeated considering the first

three and the first five modes (see table 1), and the sensitivity study is performed ranging from one to eight modes taken into account in SPA, by comparing the maximum displacement with the one obtained by applying to the available FEM a CFD loading corresponding to cruise conditions. The predicted error of SPA as a function of the number of modes is plotted in figure 5 for front and rear blades. In these figures, the dashed curve represents the SPA predicted error considering that a rectangular rosette (0°, 45°, 90°) is placed at every node in the FEM, giving an idea of the lowest error achievable.

It can be noticed for the front blade that the strain gauges pattern optimised for three modes and SPA applied taking into account three modes leads to the lowest error. For the rear blade, optimising the strain gauges pattern and applying the SPA for three or five modes gives similar results. As the front blade is mainly designed to bend and the rear blade to twist, finally the first three modes for the former and the first five modes for the latter are considered in the strain gauges pattern optimisation and when applying SPA.

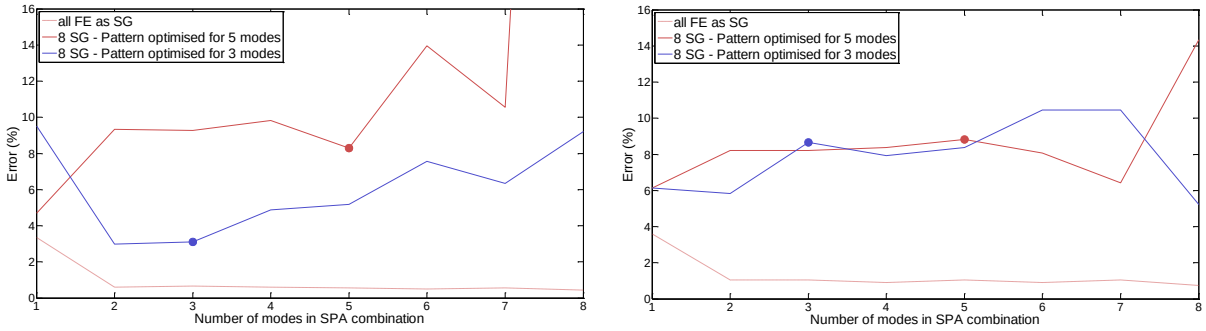

Figure 5 - SPA predicted error for reference case

4 LABORATORY TESTS

As described in section 2, a calibration phase is necessary to later apply the SPA. This phase consists in recording the modal shapes and strains for the first modes of the blades. Then, static validation and verification in rotation are performed.

A specific test set-up (SPA hub) is designed and manufactured for these operations. Mounting conditions of the blades are similar to those on the hub dedicated to wind tunnel tests. Moreover, embedded piezoelectric actuators in the test set-up allow exciting the blades in a sufficient frequency range. This test set-up, including the blades, is then installed on a rotating test bench in an ONERA laboratory, as illustrated in figure 6.

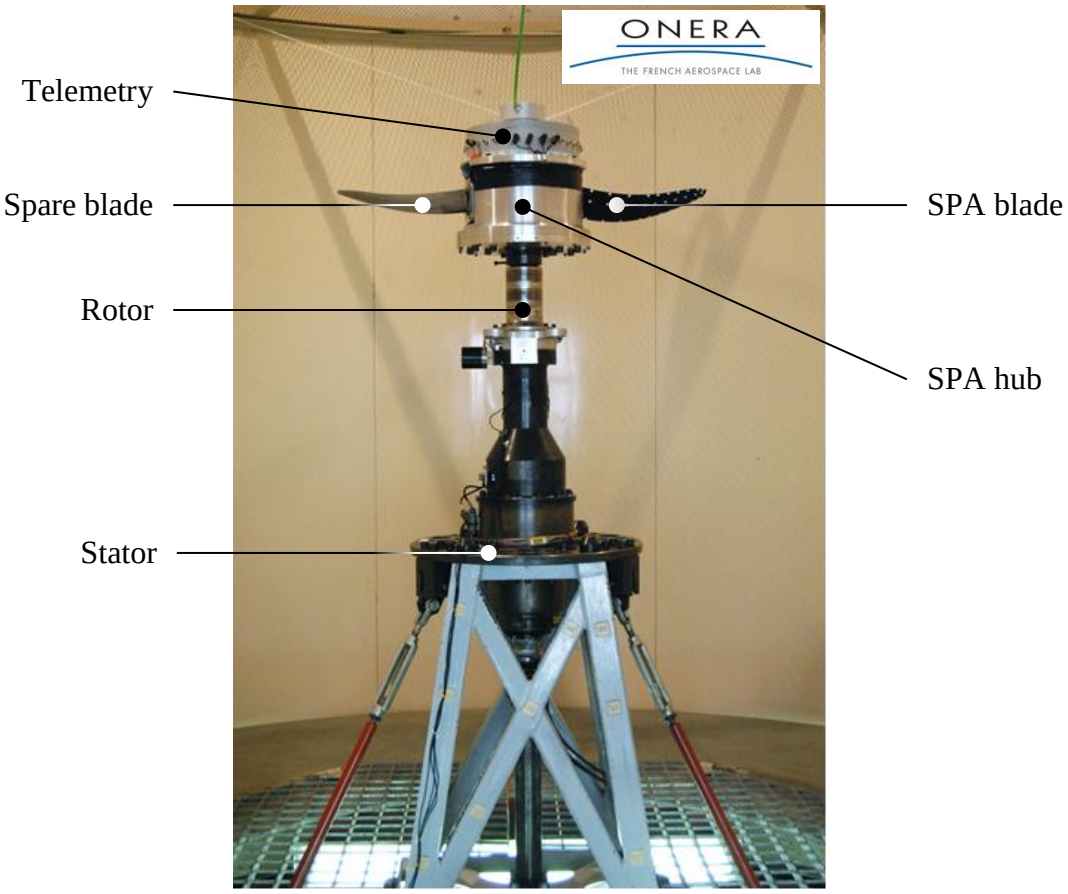

Figure 6 – Laboratory tests – Test set-up

4.1 Calibration

As explained in section 2, for front and rear blades, modal shapes and modal strains must be recorded for all modes very accurately. Quality of design and manufacturing of all parts, excitation mean, and recording system is essential to achieve this goal.

Practically, for such light structures, the modal displacements are obtained using a Laser vibrometer, in order not to influence the mechanical characteristics of the structure. Local velocities at defined locations of the structure are measured very precisely, and then local displacements are obtained by integration.

For the front SPA blade, the first three modes shapes and strains are identified. The condition number of the experimental strain matrix is equal to 3.61, which is slightly lower than estimated numerically as shown in figure 4. This demonstrates that the sensitivity of the generalised coordinates to noise, calculated as described in equation 10, is quite low. Moreover, a comparison of the experimental and numerical modal shapes is presented in figure 7, exhibiting a very good agreement for the three first modes, and consequently accrediting the optimisation of the strain gauges pattern.

Similarly, for the rear SPA blade, the first five modal shapes and strains are identified. The condition number of the experimental strain matrix is equal to 13.75. Reduced to the first three modes, it becomes equal to 3.15. It is also observed that the experimental and numerical modal shapes correlation is excellent for the three first modes, but is turning worse but still acceptable for the fourth and fifth modes.

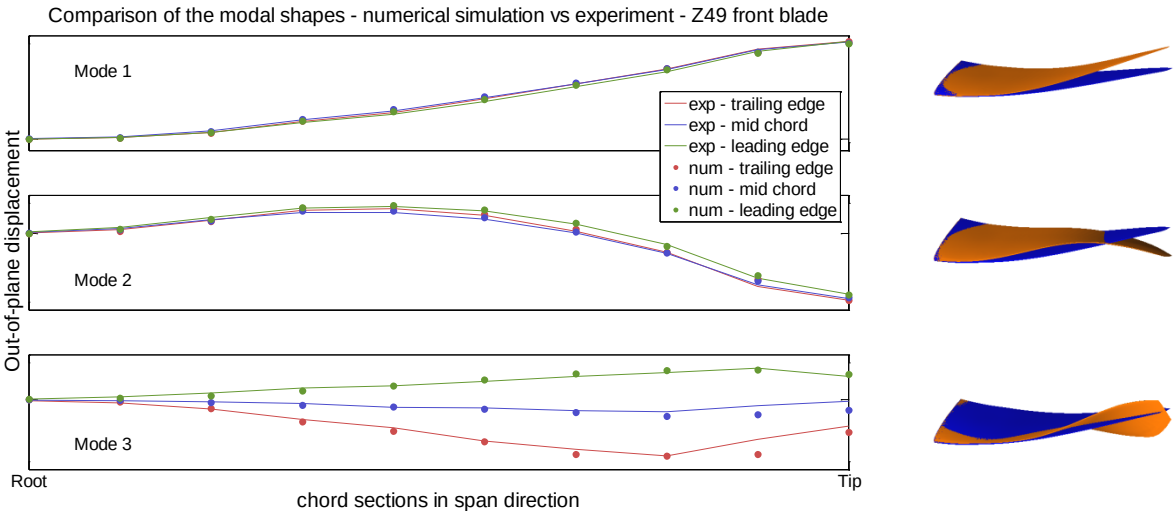

Figure 7 – Laboratory tests – Calibration of front SPA blade

4.2 Static validation

For each blade, the static validation consists in applying a distributed load, as depicted in figure 8 for the rear blade, trying to get the maximum response signals on all strain gauges full bridges. Three Keyence LK-G402 optical sensors are used to measure the blade vertical deflection simultaneously in three arbitrarily selected points, at which also SPA displacements are calculated. Time data from all signals are recorded during 60 s at 512 Hz. Application of SPA is here-below illustrated for the rear blade.

Figure 8 - Distributed loading for rear blade static validation

Moreover, it is necessary to evaluate the robustness of the SPA linear problem to a noise added to the input signals, i.e. the strain gauges full bridges signals, considering 3 or 5 modes. This aims to validate the strain gauges pattern optimisation process described in section 3.1 but also to validate the choice explained in section 3.3.3 concerning the number of modes to be taken into account for the rear blade (see figure 5). For a given number of modes, a noise (normal distribution, mean = 0, standard deviation = 1) is numerically created and added to the averaged full bridges output signals, and the SPA displacement error is calculated at the three points mentioned above. This operation is repeated 100000 times, generating three error vectors (one vector per comparison point, comprising of 100000 values). The mean values and the standard deviation of these vectors are finally calculated and plotted in figure 9 (a).

The standard deviation seems lower considering 3 modes, but the maximum or mean error that can be found on the three comparison points remains lower considering 5 modes.

Figure 9 (b) presents the whole blade deformation calculated by SPA with 5 modes (displacements are multiplied by 10 for a better visualization), in a 3D view (gray colored: undeformed shape, magenta colored: deformed shape).

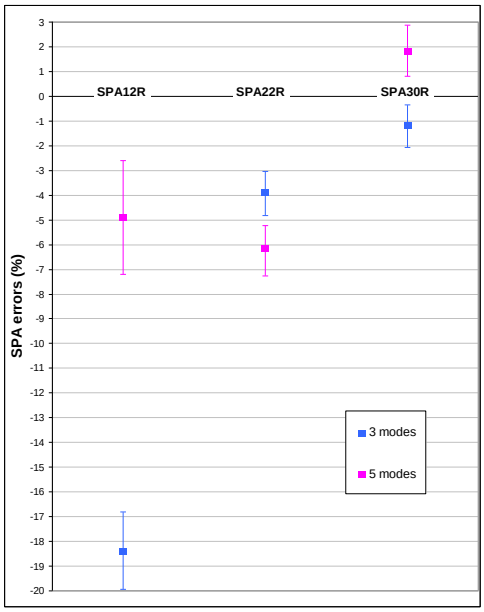

(a) SPA errors – Robustness to noise

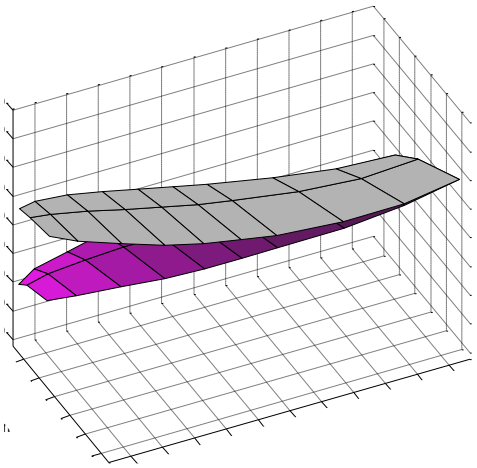

(b) SPA deflection (5 modes)

Figure 9 - Rear blade static validation

SPA is to be applied on both rear and front SPA blades during wind tunnel tests to determine theirs static and dynamic deflections, mostly at cruise condition. Unfortunately, wind tunnel test conditions are often quite more severe than laboratory conditions, and noise will be added to the signals recorded. Measuring and processing data at only one instant (time snapshot) can lead, with a low probability, to a particularly high SPA error, due to noise. Averaging prevents from getting such extreme results. In this context (considering averaging), and based on laboratory static validation, the displacement error of the SPA is about 6% for the rear blade and 5% for the front blade.

4.3 Verification in rotation

When rotating, blades are subject to centrifugal and aerodynamic forces, which tend to bend and twist them. Induced stiffening also modifies the modal frequencies, shapes and strains, as function of the rotational speed. Modal frequencies can be easily determined experimentally, analysing embedded sensors output signals, and their evolution is classically plotted in a Campbell diagram.

Modal shapes and strains recorded during calibration phase constitute the reduced basis on which SPA applies, as described by equations (6) and (8). It seems natural to wonder if this basis remains suitable when rotational speed becomes greater than 0 RPM, and how much it evolves.

For modal shapes, unfortunately, no cost-reasonable measurement system is available at the ONERA to record them directly and accurately in rotation, in laboratory.

However, with the dedicated test set-up and telemetry, we have a permanent access to strains data, with or without rotation. Thus, it is interesting to observe the modal strains at different rotational speeds.

This verification is performed in the ONERA rotating test bench, only up to 2000 RPM due to rotor balancing limitation, which is unfortunately lower than the rotational speed specified for the WTT reference case described in section 3.3. The embedded actuators make possible to excite the blades foot with sweep sinusoidal signals while the test set-up is rotating. For a fixed rotational speed, modal strains are extracted from the strains signals by calculating and signing Power Spectral Densities (PSD), eliminating aside the steady participation. For consistency, the excitation signal is always the same from a rotational speed to another.

Even if the strain gauges full bridges have been wired in order to eliminate as much as possible the centrifugal effect from the output signals, this effect can still be observed, proportionally to the rotational speed.

Arbitrarily fixing the blades pitch angle such as aerodynamic loading is not excessive but also not negligible, it is observed that the modal strains at rotation speed equal to 1000 RPM and 2000 RPM are noticeably different to the modal strains without rotation but remain almost always homothetic, as shown in table 2. Applying SPA on a new reduced basis comprising of the modal shapes without rotation (only available) and the modal strains with rotation will thus lead to almost the same final SPA displacement field. Only the generalised coordinates will be scaled.

Although being only partial, this information provides additional confidence in applying SPA in rotation.

Blade	Value	Mode 1	Mode 2	Mode 3
Rear	$MAC(S_{1000\ rpm}, S_{0\ rpm})$	0.99981	0.99989	0.99325
	$MAC(S_{2000\ rpm}, S_{0\ rpm})$	0.99879	0.9977	0.99108
Front	$MAC(S_{1000\ rpm}, S_{0\ rpm})$	0.9995	0.99982	0.99963
	$MAC(S_{2000\ rpm}, S_{0\ rpm})$	0.99265	0.9975	0.99875

Table 2 - MAC numbers of modal strains at 1000 rpm & 2000 rpm compared to modal strains at 0 rpm

5 WIND TUNNEL TESTS

5.1 Recording and pre-processing

During the WTT, time signals from SPA strain gauges full bridges are recorded by the dedicated acquisition system, as well as the front and rear propeller azimuths. The test points last 30 seconds. Before applying SPA, all signals provided are filtered with a zero-phase digital 5^{th} order Butterworth low-pass filter, cut-off frequencies being set to 1 kHz and 2 kHz for the front and rear strain signals respectively.

Rear blade strain gauges full bridge #3 signal is lost from the very beginning of the WTT campaign, with no possibility of retrieving it. By removing this signal from the SPA process, the condition number of the rear blade modal strain matrix becomes equal to 16.11, instead of 13.75 considering the 8 strain gauges full bridges, indicating that the sensibility of SPA to noise has not changed a lot.

5.2 Results

Results are required in various formats, such as images or text files, for an easy-to-read use, and in Airbus specific formats. For the sake of clarity in this paper, only images are presented. All requested values are calculated over 10s instead of 30s for time saving reason, which does not bring significant differences in the results.

Displacements are the direct results obtained by SPA. Then, twist, bending, sweep and camber quantities are derived chord per chord, respecting Airbus provided formulas.

Once these quantities calculated for each time sample, it is required to average them relatively to the azimuth. With a processed duration of 10s and for example a rotation speed of 4500 rpm, the average is made over 750 revolutions. However, for each propeller, the azimuth function of time is not perfectly linear, due to small variations of the rotational speed and the numeric precision of azimuths data in the files provided. To ease the averaging, it becomes then necessary to create a new linear function of the azimuth and to interpolate these quantities linearly at the newly generated values. An azimuthal resolution of 1° is chosen, which is a good compromise between processing time, volume of data and precision of the phenomena graphical representation.

For all test points, averages and standard deviations of variations of bending, twist, sweep and camber as function of azimuth, viewed from rear, are plotted, as illustrated partially in figure 10.

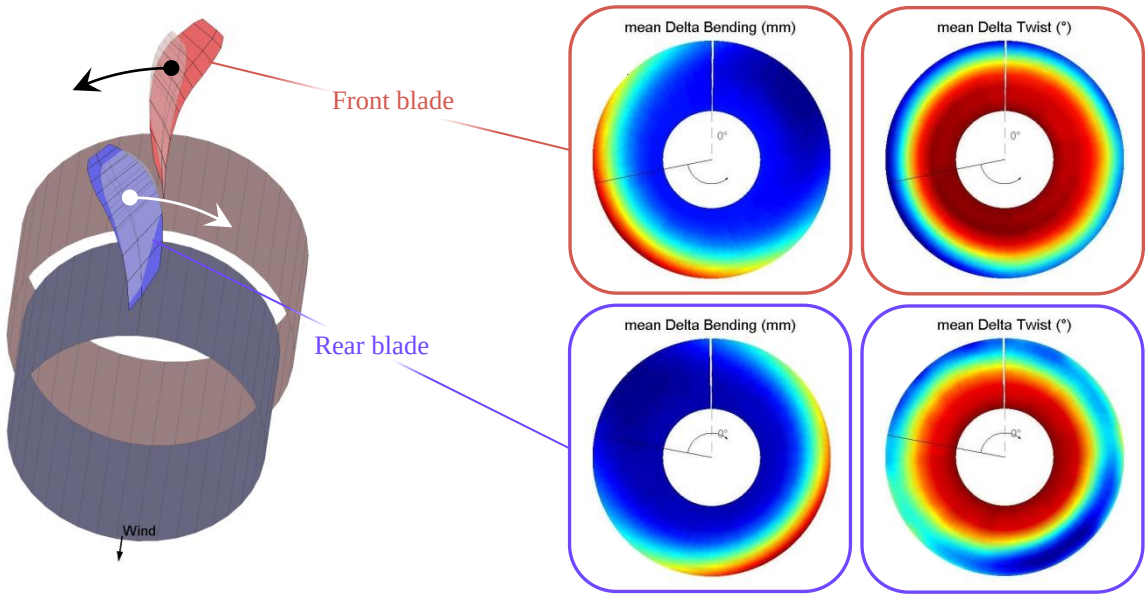

3D rear view of SPA blades Cold and hot shapes

Bending of SPA blades

Twist of SPA blades

Figure 10 – Global AoA > 0° - Averages of variations of bending and twist as function of azimuth

For test points with global Angle Of Attack (AoA) equal to zero, as loading is to be rather uniform azimuthally, variations of bending, twist, sweep and camber are also averaged over all azimuths and plotted as function of span, as shown in figure 11. These results will be conveniently used for further comparisons with high fidelity steady aeroelastic computations [7].

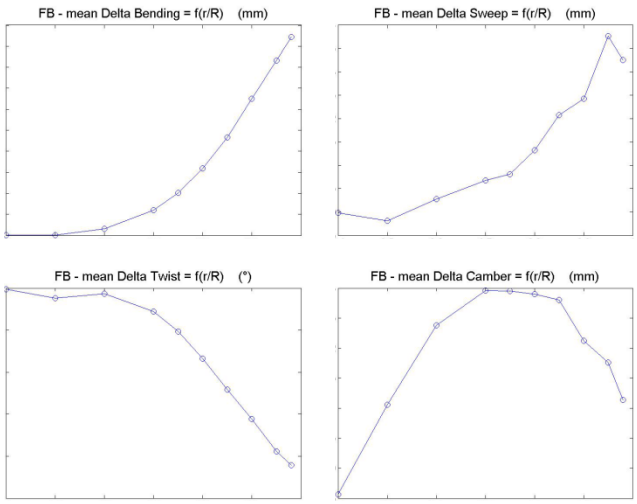

Figure 11 – Global AoA = 0° – Averages of variations of bending, twist, sweep and camber as function of span location, for the front blade

6 CONCLUSION

The SPA results delivery of Z49 wind tunnel tests concludes a long time work, started with the optimisation of strain gauges patterns. Calibration and method validation were then performed, followed by the preparation of the wind tunnel tests, these latters having finally been spread over several months.

Despite the unusuality of applying the SPA for low aspect ratio and short 3D blades, and the difficulty induced by the few sensors allowed for modes observation, results obtained during the test campaign seem to describe the aeroelastic phenomena quite well and are very encouraging. One key point among the whole work is the optimisation of the strain gauges locations, with many precautions taken right from the beginning, leading to a Strain Pattern Analysis robust enough to disturbances.

The measured blades deformations and derived quantities, as well as experimental pressure measurements, are finally dedicated to improve the high fidelity aeroelastic computational methodologies, as detailed in the companion paper [7].

7 ACKNOWLEDGMENTS

This work has been partially undertaken within the Joint Technology Initiative “JTI CleanSky”, Smart Fixed Wing Aircraft Integrated Technology Demonstrator “SFWA-ITD” project (contract N° CSJU-GAM-SFWA-2008-001) financed by the 7th Framework programme of the European Commission.

The author would like to thank mainly the Airbus Aerodynamics and Wind Tunnel Tests teams in Toulouse for supporting the application of SPA in this challenging project, as well as their permanent responsiveness, bringing all needed information when necessary.

8 REFERENCES

[1] Negulescu C., Airbus AI-PX7 CROR Design Features and Aerodynamics, *SAE int. J. Aerosp. 6(2)*, 2013, DOI:10.4271/2013-01-2245

[2] Gaukroger D.R., Hassal C. J. W., Measurement of vibratory displacements of a rotating blade, *Vertica*, vol.2, pp. 111–120.

[3] Tourjansky N., Széchényi E., The measurement of blade deflections: a new implementation of the strain pattern analysis, *13th European Rotorcraft Forum, Dearborn*, Avignon (France), Sept. 15-18, 1998.

[4] Milne R. D., Simpson A., Theoretical and numerical assessment of strain pattern analysis, *Journal of Sound and Vibration*, 1996, 192(1), pp. 349-387.

[5] Stephan C., Sensor placement for modal identification, Mechanical Systems and Signal Processing, vol.27, Feb. 2012, pp. 461-470, DOI:10.1016/j.ymssp.2011.07.022

[6] Allemang, R. J., The Modal Assurance Criterion – Twenty years of use and abuse, *Sound and Vibration*, Aug. 2003, pp. 14-21.

[7] Mauffrey Y., Geeraert A., CROR Blade deformation, part 2: Aeroelastic computations and comparison with experiments, *IFASD-2015-043*, June 2015.

9 COPYRIGHT STATEMENT